

TaCarla: A comprehensive benchmarking dataset for end-to-end autonomous driving

Tugrul Gorgulu^{1*} Atakan Dag¹ M. Esat Kalfaoglu^{2†} Halil Ibrahim Kuru¹ Baris Can Cam¹
Halil Ibrahim Ozturk¹ Ozsel Kilinc^{3‡}

Abstract

Collecting a high-quality dataset is a critical task that demands meticulous attention to detail, as overlooking certain aspects can render the entire dataset unusable. Autonomous driving challenges remain a prominent area of research, requiring further exploration to enhance the perception and planning performance of vehicles. However, existing datasets are often incomplete. For instance, datasets that include perception information generally lack planning data, while planning datasets typically consist of extensive driving sequences where the ego vehicle predominantly drives forward, offering limited behavioral diversity. In addition, many real datasets struggle to evaluate their models, especially for planning tasks, since they lack a proper closed-loop evaluation setup. The CARLA Leaderboard 2.0 challenge, which provides a diverse set of scenarios to address the long-tail problem in autonomous driving, has emerged as a valuable alternative platform for developing perception and planning models in both open-loop and closed-loop evaluation setups. Nevertheless, existing datasets collected on this platform present certain limitations. Some datasets appear to be tailored primarily for limited sensor configuration, with particular sensor configurations. Additionally, in some datasets, the expert policies used for data collection exhibit suboptimal driving behaviors, such as oscillations. To support end-to-end autonomous driving research, we have collected a new dataset comprising over 2.85 million frames using the CARLA simulation environment for the diverse Leaderboard 2.0 challenge scenarios, making it the largest dataset in the literature to the best of our knowledge. Our dataset is designed not only for planning tasks but also supports dynamic object detection, lane divider detection, centerline detection, traffic light recognition, prediction tasks and visual language action models. Furthermore, we demonstrate its versatil-

ity by training various models using our dataset. Moreover, we also provide numerical rarity scores to understand how rarely the current state occurs in the dataset.

1. Introduction

A well-curated dataset is an invaluable asset for the enhancement of machine learning research. While the task of data collection may appear straightforward, it necessitates substantial hardware resources and considerable time investment. The complexity of this process cannot be overstated, as even minor inaccuracies can compromise the integrity of the entire dataset, rendering it ineffective. The ability to measure and quantify various aspects of the data is paramount, as it directly influences the potential for model improvement. Without precise and reliable data, the iterative process of refining neural network models becomes fundamentally flawed, underscoring the critical importance of meticulous data collection and validation.

Autonomous driving continues to be a focal point of research, yet the current datasets fall short of being comprehensive. This deficiency hampers the pace of progress and results in suboptimal performance on demanding, yet realistic benchmarks such as the Carla Leaderboard 2.0 challenge, where even the most advanced approaches struggle to achieve a mere 6% success rate [37]. The inadequacy of these datasets underscores the necessity for more robust and diverse data to drive meaningful advancements in the field. Two notable datasets were released last year: Bench2Drive [18] and The PDM-Lite [3]. However, these datasets present certain limitations. Bench2Drive, the pioneering dataset for the Leaderboard 2.0 challenge, is potentially affected by oscillation issues in its expert policy. Additionally, despite collecting data for multiple tasks, Bench2Drive reports results exclusively for planning models. Similarly, the PDM-Lite dataset appears to be specifically tailored to the Transfuser planning model rather than serving as a general-purpose dataset. It employs a sensor configuration comprising three front-facing cameras and one LiDAR, precisely mirroring the setup used in the Trans-

*Corresponding author: tugrul.gorgulu@togg.com.tr

†This work was conducted at Trutek. The author is currently affiliated with Ultralytics.

‡This work was conducted at Trutek. The author is currently affiliated with Amazon.

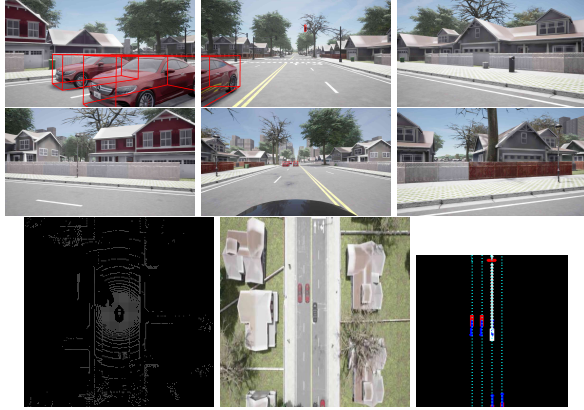


Figure 1. These images include views from 6 cameras, point cloud from LiDAR sensors, and satellite-like BEV RGB image. We visualize the ground-truth 3D bounding boxes for vehicles, and 2D bounding boxes for traffic lights on camera-view. Additionally, ground-truths are visualized on a BEV grid, including centerlines, lane guidance, and orientation for vehicles.

fuser planning model. However, this configuration is not well-suited for certain scenarios, such as the ‘YieldingEmergencyVehicle’ task in Leaderboard 2.0, where there is no input to detect an approaching emergency vehicle from behind the ego vehicle. These constraints highlight the need for more comprehensive datasets to advance research in this domain.

In pursuit of enhancing autonomous driving research, we present a novel dataset designed to elevate the performance of machine learning models in both end-to-end and modular paradigms. We seek to combine the strengths of Bench2Drive and PDM-Lite. To achieve this, we utilize the PDM model as the expert policy, leveraging its robustness and reliability. Additionally, we adopt the NuScenes sensor configuration to ensure compatibility with commonly used perception models in the literature. This approach addresses the oscillation issues observed in Bench2Drive’s expert policy and expands beyond the specific sensor setup of PDM-Lite, making our dataset more versatile and applicable to a wider range of scenarios. Moreover, our dataset supports a comprehensive range of autonomous driving tasks—such as dynamic object detection, centerline detection, traffic light recognition, prediction, and planning—which are typically adopted within the modular paradigm. Additionally, it includes tasks like 2D segmentation and depth prediction, which are essential for pretraining models in the end-to-end paradigm. This holistic approach ensures the dataset’s relevance and utility across a wide spectrum of research and practical applications. Furthermore, we have selected state-of-the-art models from the literature for each task and provided baseline performances to enable comprehensive benchmarking.

In summary, our main contributions are as follows:

- We introduce **TaCarla**, a new, large-scale dataset for the CARLA Leaderboard 2.0 challenge that addresses the gaps of previous works by providing a significantly **larger number of complex, multi-lane scenarios** requiring challenging lane-change maneuvers, as shown in Table 2.
- We **combine the strengths** of prior datasets by simultaneously using the robust **PDM expert policy** (addressing the oscillation issues found in Bench2Drive) and adopting the comprehensive **NuScenes sensor configuration** (providing the 360-degree coverage lacking in PDM-Lite).
- We provide a **holistic dataset** with rich annotations and, critically, a **comprehensive benchmark suite**. We establish robust SOTA baselines for a wide spectrum of tasks, covering both **perception components** (e.g., 3D object detection, centerline detection) and **end-to-end planning** models.
- We provide rule-based **text annotations** for each scene to support modern, LLM-based research. Furthermore, we introduce a normalized **rarity score** to quantify scenario uniqueness and help identify long-tail events in the dataset.

2. Related work

In alignment with the findings presented in [21], larger models, when trained with increased data and computational resources, consistently surpass the performance of their smaller counterparts. This phenomenon underlies the widespread adoption and success of large language models. Inspired by these insights, we aim to achieve an order of magnitude increase in dataset size for each covered task compared to existing datasets in the literature. In this section, we analyze the sizes of the widely adopted datasets in autonomous driving and evaluate the range of tasks they address.

Dynamic object detection. Dynamic object detection remains one of the foremost challenges in autonomous driving. The KITTI Object Detection Dataset [12], introduced in 2017, was specifically developed for 3D object detection and comprises 7,481 training images and 7,518 test images, encompassing a total of 80,256 labeled objects. The Waymo Open Dataset for perception tasks [41], last updated in 2024, includes 390,000 frames for 3D object detection. The nuScenes dataset [4], released in 2021, features 1.4 million 3D bounding boxes and is widely regarded as one of the most popular datasets for dynamic object detection. Argoverse 2 [45], released in 2023, contains 150,000 samples. The nuPlan dataset [22], released in 2023 originally for planning, includes approximately 120 hours of raw sensor data with autolabeled ground-truths.

2D Lane Detection. The 2D Lane Detection task aims to detect lane dividers from Perspective View (PV) and project them to a Bird’s Eye View (BEV) under the flat world assumption. The TuSimple dataset [50], launched in 2017, contains 3,626 images in the training set, 358 in the validation set, and 2,782 in the test set. The CULane dataset [33], released in 2018, comprises 133,235 frames, meticulously divided into 88,880 for the training set, 34,680 for the test set, and 9,675 for the validation set. However, both CULane and TuSimple datasets contain only four to five lane dividers, which limits the completeness of lane divider detection. The BDD100K dataset [52], released in 2020, comprises 100,000 labeled images. The CurveLanes dataset [47], published in 2020, includes 150,000 frames, with 100,000 allocated for training, 20,000 for validation, and 30,000 for testing. The Curvelanes dataset is important from the perspective that it includes high curvature lane dividers and includes up to 9 instances. Published in 2021, the VIL100 dataset [55] includes 10,000 frames. The CARLANE dataset [40], released in 2022, is another dataset collected using Carla Simulation, focusing primarily on lane detection, and includes 84,000 images.

3D Lane Detection. The 3D Lane Detection task aims to detect the 3D Lane coordinates of lane dividers directly. These datasets address the limitation of flat world assumption in 2D lane detection datasets. Introduced in 2019, the LLamas dataset [2] encompasses a total of 100,000 annotated images. Published in 2020, the Gen-LaneNet dataset [13] is a synthetic dataset and contains 6,000 samples. The KLane dataset [32], released in 2021, includes 15,000 frames of real images. The Once-3DLanes dataset [48], released in 2022, includes 211,000 simulated samples. The OpenLane-V1 dataset [6], launched in 2022, comprises 200,000 frames, offering a substantial resource for lane detection research. The LanEvil dataset [54], published in 2024, was generated using the CARLA simulator and contains 90,292 images.

Centerline and Topology Dataset. The OpenLane-V2 dataset [44], launched in 2024, comprises two distinct subsets, offering a comprehensive resource for lane detection research. Subset-A, derived from Argoverse V2, includes 22,477 training samples, 4,806 validation samples, and 4,816 test samples, with a resolution of 2048x1550. Subset-B, derived from NuScenes, contains 27,968 training samples, 6,019 validation samples, and 6,008 test samples, with a resolution of 1600x900.

Traffic Light Detection. Traffic light detection involves identifying 2D bounding boxes around traffic lights and determining their classes. This specialized task requires more

detailed information and larger datasets than generic object detection [11, 14, 24, 30]. The LISA Traffic Light Dataset [35] includes 46,418 frames and 112,971 annotated traffic lights with 7 classes. The BOSCH Small Traffic Light Dataset [1] has 13,427 images and approximately 24,000 annotated traffic lights. BDD100K [51] provides 100,000 driving videos and 14,606 annotated traffic lights, supporting various vision tasks for autonomous driving. Unlike these datasets, our contribution aligns traffic light data with other sensory inputs (LIDAR, Ego Status) and driving waypoint information.

Planning. The aim of the planning task is to generate waypoints for the ego-vehicle to navigate to its destination while addressing complex challenges. Several datasets have been developed to address this problem. The NuPlan dataset [22], comprising 1,200 hours of driving data, is one of the pioneering benchmarks in this domain. It includes dynamic objects, traffic lights on the HD map, and lane information from the HD map. However, a significant limitation of the NuPlan dataset is its lack of diversity in planning tasks, as a large portion of the data involves the ego vehicle merely moving forward [8, 15, 53]. The Bench2Drive dataset [18], released for the Leaderboard 2.0 challenge in 2024, contains 2 million frames collected at 10 Hz using a reinforcement learning (RL)-based expert that leverages ground truth information from the CARLA simulation. A drawback of this dataset is the potential for oscillation issues in the ego vehicle, which can affect its behavior in scenarios—a common problem in RL agents [5, 31]. In our dataset, the PDM-Lite rule-based expert was used to collect the data. The PDM-Lite dataset, published in 2024, was created using the PDM-Lite rule-based expert. It contains 581,662 samples, collected at a frequency of 4 Hz. However, this dataset is limited by its sensor configuration. In contrast, our dataset utilizes one of the popular sensor configurations from the NuScenes dataset [4], allowing for a seamless switch between the two.

3. TaCarla

Samples of the TaCarla dataset were meticulously collected based on training and validation routes provided by the Leaderboard 2.0 challenge in the CARLA 0.9.15 simulation. The Leaderboard 2.0 encompasses 36 distinct scenarios, including lane changing at the appropriate time, interacting with pedestrians, prioritizing emergency vehicles, managing traffic lights, and responding to unexpected stops of nearby vehicles, among others, to emulate real-life traffic situations. Detailed descriptions of these scenarios are provided in the Appendices. To demonstrate the diversity of trajectories in our dataset, we compare it with nuScenes [4] and Bench2Drive [18] in Figure 2, in a similar fashion to

the comparison provided in Bench2Drive [18]. This comparison illustrates that our data collection expert can execute more diverse movements over extended distances. Our heatmap, depicting trajectories over a 4-second horizon, indicates that our vehicle can reach speeds of up to 72 km/h, thereby showcasing the diversity in velocity as well.

Given the multitude of scenarios in the XML files, we meticulously separated them into distinct routes based on the trigger points where each scenario is executed. This separation was performed between two consecutive scenarios on the original routes. The dataset comprises over 2,850,000 frames recorded at 10 Hz under various weather conditions, utilizing the NuScenes sensor configuration, which is one of the most widely used setups for perception tasks. Therefore, akin to the NuScenes dataset, our dataset incorporates 6 RGB cameras, 5 radars, and 1 LiDAR sensor, all positioned identically to those in NuScenes. In addition to these sensors, we also collect bird’s-eye view RGB images (reminiscent of satellite imagery), depth camera data, instance segmentation images, and semantic segmentation images, as these modalities are extensively utilized in perception research. Furthermore, depth, instance segmentation, and semantic segmentation images are captured using the same camera configuration, aligning with common practices in the literature for perception tasks.

The dataset encompasses seven distinct object types, categorized based on their significance in planning scenarios. These categories include *walker*, *car*, *police*, *ambulance*, *firetruck*, *crossbike*, and *construction*. Specifically, the dataset comprises 67,985 walkers, 7,939,572 cars, 115,022 police vehicles, 9,442 ambulances, 3,972 firetrucks, 119,165 crossbikes, and 427,622 construction objects. Additionally, there are 238,780 traffic light samples in Town12 and 187,987 in Town13.

The TaCarla dataset includes environmental information such as initial weather conditions stored in the `simulation_results` in the corresponding parquet file. The key weather parameters are *cloudiness*, *fog_density*, *precipitation*, *precipitation_deposits*, and *wetness*. Each parameter ranges from 0 to 100.

In Table 1, to improve interpretability, these numerical values are grouped into categories: *very_low_effect* (0–20), *low_effect* (20–40), *medium_effect* (40–80), and *heavy_effect* (80–100).

Table 1. Weather Condition Distributions in the TaCarla Dataset

Condition	Clean (%)	Low (%)	Medium (%)	Heavy (%)
Cloudiness	35.49	7.65	34.22	22.62
Fog Density	68.45	3.31	23.82	4.40
Precipitation	51.77	3.76	33.99	10.46
Precipitation Deposits	33.65	3.37	49.16	13.80
Wetness	79.87	0.41	10.79	8.91

In some scenarios, such as Accident, AccidentTwoWays, ConstructionObstacle, ConstructionObstacleTwoWays,

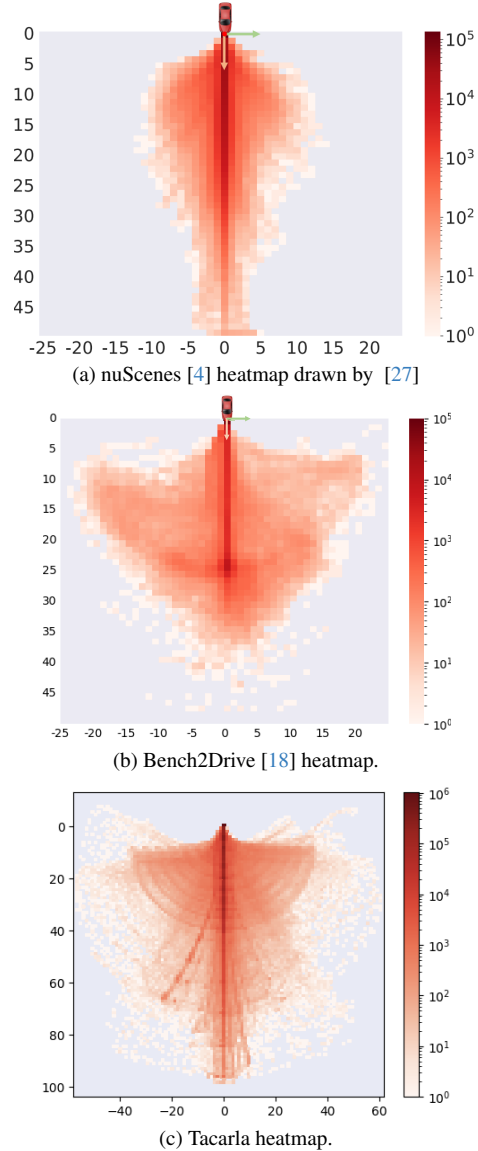


Figure 2. Distribution of the ego vehicle’s ground-truth location.

HazardAtSideLane, HazardAtSideLaneTwoWays, ParkedObstacle, ParkingCrossingPedestrian, ParkingExit, and YieldToEmergencyVehicle, the ego vehicle needs to change lanes to accomplish the scenario. Therefore, it must observe not only the vehicle in front of it but also other vehicles in adjacent lanes. Consequently, these scenarios are more complex than the rest. The comparison of scenarios in TaCarla, Bench2Drive, and PDM-Lite is presented in Table 2. It can be observed that the number of such tasks in TaCarla significantly exceeds those in the other datasets. The details of these scenarios can be found in the Appendix.

Since large language models (LLMs) have become very prevalent recently, many researchers have started incorpo-

Table 2. Number of scenarios in TaCarla compared to Bench2Drive and PDM-Lite

Scenario	TaCarla	Bench2Drive	PDM-Lite
Accident	353	28	88
AccidentTwoWays	410	201	97
BlockedIntersection	43	582	96
ConstructionObstacle	306	27	92
ConstructionObstacleTwoWays	310	138	94
ControlLoss	255	18	266
CrossingBicycleFlow	153	105	50
DynamicObjectCrossing	452	26	266
EnterActorFlow	71	19	112
HardBreakRoute	281	35	96
HazardAtSideLane	123	187	78
HazardAtSideLaneTwoWays	358	27	97
HighwayCutIn	144	39	83
HighwayExit	28	29	88
InterurbanActorFlow	10	13	92
InterurbanAdvancedActorFlow	79	42	84
MergerIntoSlowTraffic	118	71	173
NonSignalizedJunctionLeftTurn	308	116	99
NonSignalizedJunctionRightTurn	391	156	91
OppositeVehicleRunningRedLight	385	85	261
OppositeVehicleTakingPriority	231	614	99
ParkedObstacle	261	28	93
ParkedObstacleTwoWays	416	23	90
ParkingCrossingPedestrian	338	20	90
ParkingCutIn	259	38	96
ParkingExit	132	27	98
PedestrianCrossing	188	215	99
PriorityAtJunction	492	116	94
SignalizedJunctionLeftTurn	185	21	327
SignalizedJunctionRightTurn	213	15	237
StaticCutIn	230	24	100
VehicleTurningRoute	124	235	584
VehicleTurningRoutePedestrian	87	18	98
YieldToEmergencyVehicle	268	19	84

rating them into autonomous driving tasks to enhance reasoning abilities of AI models. Therefore, in this study, we also generate textual descriptions that provide information about the current scene of the ego vehicle. These text annotations were extracted using a rule-based approach that leverages the 3D labels of lanes, objects, and lane guidance in our dataset.

In addition, the CARLA Leaderboard 2.0 challenge includes many edge-case scenarios. However, as shown in the distributions in Figure 2, the ground truths for simply following the route and going straight are overrepresented in all three datasets. As one might expect, this can lead to an imbalance in the datasets, as the ego vehicles may not effectively learn other behaviors. To quantify this imbalance and identify rare events, we propose a **rarity score** applicable to any dataset containing text annotations. This score adapts the Inverse Document Frequency (IDF) [39] to measure the uniqueness of a given text annotation W_t (representing the current scenario) relative to the entire corpus N . The score is calculated as:

$$\text{Rarity}(W_t) = \frac{1}{|W_t|} \sum_{w \in W_t} \log \left(\frac{1 + l_N}{1 + \sum_{n \in N} \mathbf{1}_{\{w \in n\}}} \right)$$

$$\text{FinalRarity}(W_t) = \frac{\text{Rarity}(W_t) - \min(\text{Rarity})}{\max(\text{Rarity}) - \min(\text{Rarity})}$$

where $\text{Rarity}(W_t)$ represents the unnormalized rarity value of the current text W_t , and $\min(\text{Rarity})$ and $\max(\text{Rarity})$ denote the minimum and maximum rarity scores observed across the entire dataset. This normalization maps all rarity values into the range $[0, 1]$, where higher values indicate rarer or more distinctive textual descriptions.

In this formula, l_N is the total number of sentences (corpus length), W_t is the current sentence being scored, w is a word in W_t , n is any sentence in the corpus N , and $\mathbf{1}_{\{\cdot\}}$ is the indicator function.

Empirically, this score effectively distinguishes common from rare events. As illustrated in Figure 3, common route-following scenarios register a low score (approx. 0.0), whereas the score increases significantly for more complex or unusual situations.

4. Experiments

4.1. 3D Object Detection

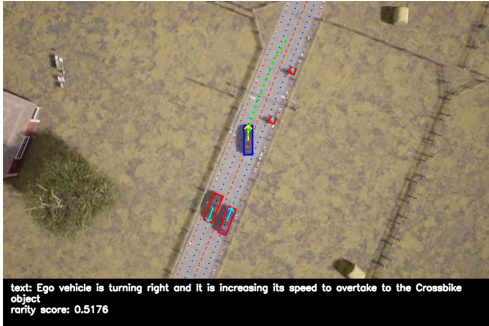
We employed a non-transformer-based architecture for multi-view bird’s eye view (BEV)-based 3D object detection. In this architecture, the multi-view camera images are initially processed by a convolutional image encoder, specifically RegNetY-800MF [36], with a feature pyramid network based on BiFPN [42]. We project the feature levels at /8, /16, and /32 resolutions into the BEV representation using Lift-Splat projection [34]. Features from the previous two frames are warped to the current frame using egomotion and then concatenated along the channel dimension, similar to BevDet4D [17]. Gradients produced by the previous frames are not used to update the image encoder. The resulting spatio-temporal BEV features are processed by a ResNet-based [16] BEV backbone. These features are then shared among task-specific heads. We utilize RQR3D [23] for BEV-based 3D object detection. RQR3D reparametrizes the regression targets for the 3D bounding boxes and implements this reparameterized regression task on an anchor-free single-stage object detector, introducing an objectness head to address class imbalance problems of single-stage object detectors. RQR3D outperforms widely-adopted CenterPoint-based approaches [49], yielding lower translation and orientation errors, which are crucial for safe autonomous driving. When using LiDAR, we simply map the point cloud onto the BEV grid and concatenate it with the projected image feature before temporal processing.



(a) The ego vehicle is just following the route.



(b) The ego vehicle is slowing down because of another car.



(c) The ego vehicle is overtaking the bicycles.

Figure 3. Outputs of the TaCarla Label Viewer

To align our dataset with the nuScenes [4] benchmark, which provides annotated keyframes at 2 Hz, we downsample our original 10 Hz data to 2 Hz. This conversion ensures consistency in temporal resolution, facilitating fair comparisons and compatibility with existing evaluation protocols. Additionally, we select the scenarios whose name contains keywords such as *accident*, *construction*, *dynamic*, *pedestrian*, *hazard*, *emergency*, and *opposite* in order to achieve a more balanced class distribution.

We utilize two different sensor configurations: camera-only and camera-LiDAR. Evaluation metrics are adopted from nuScenes [4], including mean Average Precision (mAP), Average Translation Error (ATE), Average Scale Error (ASE), Average Orientation Error (AOE) and Average Velocity Error (AVE), excluding Average Attribute Er-

Table 3. Camera-only 3D object detection performance.

	AP	ATE	ASE	AOE	AVE
Car	0.459	0.444	0.147	0.012	0.559
Crossbike	0.324	0.242	0.094	0.057	0.165
Walker	0.426	0.456	0.885	1.333	0.292
Police	0.381	0.249	0.056	0.011	0.048
Construction	0.419	0.665	0.812	1.125	0.065
Ambulance	0.098	0.440	0.132	0.065	0.525
Firetruck	0.140	0.487	0.155	0.004	0.618
Mean	0.32	0.43	0.33	0.37	0.32

Table 4. Camera-LiDAR 3D object detection performance.

	AP	ATE	ASE	AOE	AVE
Car	0.716	0.173	0.125	0.022	0.399
Crossbike	0.556	0.113	0.086	0.076	0.119
Walker	0.527	0.152	0.885	1.304	0.277
Police	0.486	0.082	0.052	0.018	0.038
Construction	0.657	0.253	0.821	1.125	0.098
Ambulance	0.428	0.254	0.100	0.074	0.283
Firetruck	0.452	0.270	0.108	0.002	0.344
Mean	0.55	0.19	0.31	0.37	0.22

Table 5. Centerline and Lane Divider Detection Results of TopoBDA architecture for TaCarla Dataset.

Detection Task	AP _f	AP _c	F1 _{1.5}
Centerline Detection	39.6	41.7	67.3
Lane Divider Detection	N/A	32.1	64.3

ror (AAE) as it is not applicable for TaCarla. These metrics provide a comprehensive assessment of detection performance across various object classes. The inclusion of LiDAR modality enhances depth estimation accuracy, leading to improved localization and orientation predictions, as reflected in lower ATE and AOE values. Conversely, the camera-only configuration exhibits higher errors due to the inherent challenges in depth estimation. The detailed class-wise performance metrics are presented in Tables 3 and 4, illustrating the comparative effectiveness of both training approaches.

4.2. Lane Detection

Lane detection consists of two sub-tasks which are lane divider detection and centerline detection. For the lane divider and centerline detection tasks, Chamfer Distance-based Average Precision (AP_c) [25, 29] and Frechet Distance-based Average Precision (AP_f) [26, 44, 46] met-

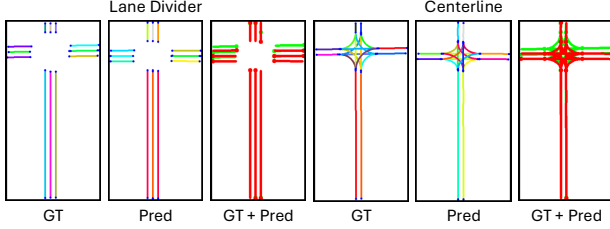


Figure 4. Bird’s Eye View (BEV) results demonstrating the performance of TopoBDA on the TaCarla dataset. GT denotes the ground truth, and Pred denotes the predictions. GT + Pred shows the overlaid results of both, facilitating visual assessment of localization performance.

rics were utilized. These metrics are commonly used in the literature to evaluate the geometric similarity between predicted and ground-truth polylines. For AP_f , the thresholds are 1, 2, and 3 meters, and for AP_c , the thresholds are 0.5, 1, and 1.5 meters. Additionally, the F1 metric is included, which is another widely used metric in the literature for assessing lane detection performance [6, 13]. In the F1 metric calculation, if 75% of the points are within the predetermined threshold, the instances are assumed to be true positives. In this study, this threshold is set to 1.5 meters, in accordance with the literature. For all evaluation metrics, 11 ground truth points are utilized.

For the training of both centerlines and lane dividers, the TopoBDA study [19] was utilized, which incorporates specialized attention structures and advanced polyline training practices derived from the TopoMaskV2 study [20]. The Bezier Deformable Attention mechanism, a key innovation of TopoBDA, focuses attention around Bezier keypoints rather than a single central point. This approach enhances the efficiency of polyline learning by improving the detection and representation of elongated and thin polyline structures.

The results for the training of TopoBDA for lane divider and centerline detection are presented in Table 5. The experimental details for this training are consistent with those outlined in the TopoBDA study [19] except that the training duration is set to 6 epochs. The Frechet Distance-based Average Precision (AP_f) is marked as N/A because the Frechet distance emphasizes directional information, which is not relevant to the lane divider detection task. In the experiments, the TaCarla dataset is utilized in a 2Hz configuration, and the validation set is subsampled further with a factor of 5.

Bird’s Eye View (BEV) demonstrations are presented in Figure 4, respectively. These figures include visualizations of both centerlines and lane dividers. In the figure, GT denotes the ground truth, while Pred represents the predictions made by TopoBDA. Additionally, Figure 4 includes an overlaid visualization (GT + Pred), which aids in un-

derstanding the localization performance. It is noteworthy that in junction regions, lane dividers are excluded, whereas centerlines are included, as illustrated in Figure 4.



Figure 5. Outputs of the FCOS traffic light model

4.3. Traffic Light Detection

The dataset we propose consists of 238,780 and 187,987 images containing traffic light instances in the training and validation sets, respectively. Every individual image in the dataset consists of a traffic light instance with three distinct classes: *red*, *yellow*, *green*. Every instance is labeled with its 2D bounding box and corresponding class. For the traffic light detection task, we employed off the shelf single-stage object detector FCOS [43] with ResNet-50 backbone as a baseline. We use a 1x training schedule; we train for 12 epochs with a learning rate of $1e^{-3}$. We schedule the learning rate at 8th and 11th epochs with a rate of 0.1. We report COCO style [30] AP and AP_{50} in Table 6.

Table 6. Traffic Light Detection task results in TaCarla.

Model	AP	AP_{50}
FCOS [43]	59.5	88.2

4.4. Planning

For the planning task, we trained three baseline agents: Transfuser [7], DiffusionDrive [28], and PlanT [38]. We choose Transfuser and DiffusionDrive upon their great success in the Navsim [9] dataset. Both agents were trained with the same Resnet-34 backbone [16], which uses 3 forward-facing cameras and LiDAR. The cameras are cropped and concatenated as a single image of size 256×1024 and LiDAR point clouds rasterized with a BEV

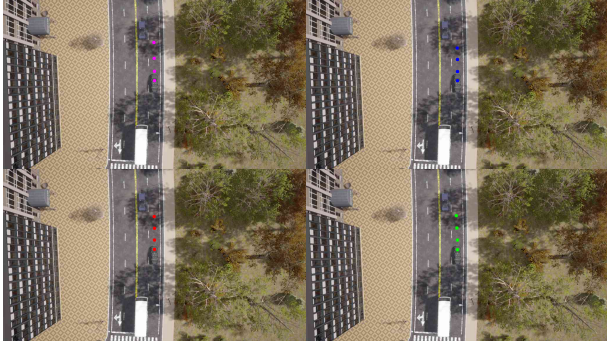


Figure 6. Waypoints from ground truth(Top Left), PlanT(Top Right), Transfuser(Bottom Left), and DiffusionDrive (Bottom Right) models.

Table 7. Open-loop results on the validation set of unseen Town13 with 1s, 2s, and 4s planning horizons (H).

Model	\mathcal{H}	ADE	FDE	AHE	FHE
DiffusionDrive [28]	4	2.69	5.58	0.27	0.21
	2	1.14	2.14	0.21	0.21
	1	0.51	0.78	0.12	0.12
PlanT [38]	4	-	-	-	-
	2	1.03	1.71	0.36	0.34
	1	-	-	-	-
Transfuser [7]	4	2.29	4.97	0.23	0.27
	2	0.91	1.74	0.23	0.27
	1	0.40	0.59	0.22	0.22

size 256×256 . Both agents use the same ego status input, which consists of vector velocity, acceleration, and driving command. The driving command is calculated as it is in Navsim [9]. We used our annotated lane guidance waypoints by classifying the point 15m away from the ego position as left, right, or straight by checking the lateral distance with a threshold of 2m. We trained DiffusionDrive for 6 epochs and Transfuser for 3 epochs with a learning rate of 7.5×10^{-5} on 8 NVIDIA A100 GPUs with a total batch size of 64. We filtered our training set scenarios with a driving score ≥ 70 . During training, we sampled ground truth trajectories with 2Hz, which gives 8 waypoints for a 4 seconds horizon. The implementation architecture is the same with DiffusionDrive paper [28], where we used 20 anchors clustered from our dataset. During evaluation, we used 2 denoising steps as the authors used in the Navsim challenge [9]. The other chosen planning model was the PlanT model [38] because it is one of the best planning models that utilizes ground truth information. We trained the PlanT model for 50 epochs, with a batch size of 16 and a learning rate of 10^{-4} .

For the evaluation of the trained agents, we provide both

open-loop and closed-loop results. Open-loop results are calculated by computing the average displacement error (ADE), the final displacement error (FDE), the average head error (AHE), and the final head error (FHE) between the predicted and ground-truth trajectories as it is calculated in NuPlan [22]. We provide our metrics for 3 different prediction horizons in seconds with 2Hz sampling rate. We used the Town13 validation set of our dataset. See Table 7 for the results. For the closed-loop evaluation, we simplified our validation dataset routes to 36 scenarios and run them with the CARLA Leaderboard V2 [10] framework. We provide scenario-specific open-loop and closed-loop results in the Appendix.

4.5. Evaluation Results of Planning Agents

Closed-loop metrics are summarized in Table 8. These metric scores were obtained using leaderboard 2.0 original metrics in the challenge. The routes of the scenarios are randomly selected in Town13 scenarios in Leaderboard 2.0.

Table 8. Closed-loop metrics in unseen Town13 (Driving Score \uparrow , Route Score \uparrow , Penalty \uparrow) on validation routes. PlanT* is trained with the samples whose corresponding rarity scores are greater than 0.

Model	Driving	Route	Penalty
DiffusionDrive [28]	22.35	62.06	0.339
Transfuser [7]	17.18	65.67	0.283
PlanT [38]	52.95	81.67	0.658
PlanT* [38]	59.25	81.59	0.705

5. Conclusion

In conclusion, while the field of autonomous driving research has made significant strides, the limitations of existing datasets impede progress, particularly in challenging environments like the Carla Leaderboard 2.0. Current datasets, such as Bench2Drive [18] and PDM-Lite [3], while valuable, reveal shortcomings that restrict their generalizability and performance across a wide range of tasks. These gaps highlight the pressing need for more diverse and adaptable data to foster advancements in autonomous driving. In response to this challenge, we have developed a new dataset that integrates the strengths of previous efforts, including the robust PDM model and the versatile NuScenes [4] sensor configuration. This dataset is designed to address existing limitations, offering broad applicability across both end-to-end and modular systems. By incorporating a comprehensive set of tasks, ranging from dynamic object detection to traffic light recognition and depth prediction, our dataset aims to support cutting-edge research and improve model performance across various domains.

References

- [1] Karsten Behrendt and Libor Novak. A deep learning approach to traffic lights: Detection, tracking, and classification. In *Robotics and Automation (ICRA), 2017 IEEE International Conference on*. IEEE, 2017. 3
- [2] Karsten Behrendt and Ryan Soussan. Unsupervised labeled lane markers using maps. In *Proceedings of the IEEE International Conference on Computer Vision*, 2019. 3
- [3] Jens Beißwenger. PDM-Lite: A rule-based planner for carla leaderboard 2.0. <https://github.com/OpenDriveLab/DriveLM/blob/DriveLM-CARLA/docs/report.pdf>, 2024. 1, 8
- [4] Holger Caesar, Varun Bankiti, Alex H Lang, Sourabh Vora, Venice Erin Liong, Qiang Xu, Anush Krishnan, Yu Pan, Giancarlo Baldan, and Oscar Beijbom. nuscenes: A multi-modal dataset for autonomous driving. In *Proceedings of the IEEE/CVF conference on computer vision and pattern recognition*, pages 11621–11631, 2020. 2, 3, 4, 6, 8
- [5] Chen Chen, Hongyao Tang, Jianye Hao, Wulong Liu, and Zhaopeng Meng. Addressing action oscillations through learning policy inertia, 2021. 3
- [6] Li Chen, Chonghao Sima, Yang Li, Zehan Zheng, Jiajie Xu, Xiangwei Geng, Hongyang Li, Conghui He, Jianping Shi, Yu Qiao, and Junchi Yan. Persformer: 3d lane detection via perspective transformer and the openlane benchmark. In *European Conference on Computer Vision (ECCV)*, 2022. 3, 7
- [7] Kashyap Chitta, Aditya Prakash, Bernhard Jaeger, Zehao Yu, Katrin Renz, and Andreas Geiger. Transfuser: Imitation with transformer-based sensor fusion for autonomous driving. *Pattern Analysis and Machine Intelligence (PAMI)*, 2023. 7, 8
- [8] Kashyap Chitta, Daniel Dauner, and Andreas Geiger. Sledge: Synthesizing driving environments with generative models and rule-based traffic, 2024. 3
- [9] Daniel Dauner, Marcel Hallgarten, Tianyu Li, Xinshuo Weng, Zhiyu Huang, Zetong Yang, Hongyang Li, Igor Gilitschenski, Boris Ivanovic, Marco Pavone, Andreas Geiger, and Kashyap Chitta. Navsim: Data-driven non-reactive autonomous vehicle simulation and benchmarking. In *Advances in Neural Information Processing Systems (NeurIPS)*, 2024. 7, 8
- [10] Alexey Dosovitskiy, German Ros, Felipe Codevilla, Antonio Lopez, and Vladlen Koltun. CARLA: An open urban driving simulator. In *Proceedings of the 1st Annual Conference on Robot Learning*, pages 1–16, 2017. 8
- [11] M. Everingham, L. Van Gool, C. K. I. Williams, J. Winn, and A. Zisserman. The pascal visual object classes (voc) challenge. *International Journal of Computer Vision (IJCV)*, 88(2):303–338, 2010. 3
- [12] Andreas Geiger, Philip Lenz, and Raquel Urtasun. Are we ready for autonomous driving? the kitti vision benchmark suite. In *Conference on Computer Vision and Pattern Recognition (CVPR)*, 2012. 2
- [13] Yuliang Guo, Guang Chen, Peitao Zhao, Weide Zhang, Jinghao Miao, Jingao Wang, and Tae Eun Choe. *Gen-LaneNet: A Generalized and Scalable Approach for 3D Lane Detection*, page 666–681. Springer International Publishing, 2020. 3, 7
- [14] Agrim Gupta, Piotr Dollar, and Ross Girshick. Lvis: A dataset for large vocabulary instance segmentation. In *The IEEE Conference on Computer Vision and Pattern Recognition (CVPR)*, 2019. 3
- [15] Marcel Hallgarten, Julian Zapata, Martin Stoll, Katrin Renz, and Andreas Zell. Can vehicle motion planning generalize to realistic long-tail scenarios?, 2024. 3
- [16] Kaiming He, Xiangyu Zhang, Shaoqing Ren, and Jian Sun. Deep residual learning for image recognition. In *2016 IEEE Conference on Computer Vision and Pattern Recognition (CVPR)*, pages 770–778, 2016. 5, 7
- [17] Junjie Huang and Guan Huang. Bevdet4d: Exploit temporal cues in multi-camera 3d object detection. *arXiv preprint arXiv:2203.17054*, 2022. 5
- [18] Xiaosong Jia, Zhenjie Yang, Qifeng Li, Zhiyuan Zhang, and Junchi Yan. Bench2drive: Towards multi-ability benchmarking of closed-loop end-to-end autonomous driving. In *NeurIPS 2024 Datasets and Benchmarks Track*, 2024. 1, 3, 4, 8
- [19] Muhammet Esat Kalfaoglu, Halil Ibrahim Ozturk, Ozsel Kilinc, and Alptekin Temizel. Topobda: Towards bezier deformable attention for road topology understanding. *arXiv preprint arXiv:2412.18951*, 2024. 7
- [20] Muhammet Esat Kalfaoglu, Halil Ibrahim Ozturk, Ozsel Kilinc, and Alptekin Temizel. Topomaskv2: Enhanced instance-mask-based formulation for the road topology problem. *arXiv preprint arXiv:2409.11325*, 2024. 7
- [21] Jared Kaplan, Sam McCandlish, Tom Henighan, Tom B. Brown, Benjamin Chess, Rewon Child, Scott Gray, Alec Radford, Jeffrey Wu, and Dario Amodei. Scaling laws for neural language models, 2020. 2
- [22] Napat Karnchanachari, Dimitris Geromichalos, Kok Seang Tan, Nanxiang Li, Christopher Eriksen, Shakiba Yaghoubi, Noushin Mehdipour, Gianmarco Bernasconi, Whye Kit Fong, Yiluan Guo, and Holger Caesar. Towards learning-based planning: The nuplan benchmark for real-world autonomous driving. In *2024 IEEE International Conference on Robotics and Automation (ICRA)*, pages 629–636, 2024. 2, 3, 8
- [23] Ozsel Kilinc and Cem Tarhan. Rqr3d: Reparametrizing the regression targets for bev-based 3d object detection. 2025. 5
- [24] Alina Kuznetsova, Hassan Rom, Neil Alldrin, Jasper R. R. Uijlings, Ivan Krasin, Jordi Pont-Tuset, Shahab Kamali, Stefan Popov, Matteo Mallocci, Tom Duerig, and Vittorio Ferrari. The open images dataset V4: unified image classification, object detection, and visual relationship detection at scale. *arXiv e-prints:1811.00982*, 2018. 3
- [25] Qi Li, Yue Wang, Yilun Wang, and Hang Zhao. Hdmapnet: An online hd map construction and evaluation framework. In *2022 International Conference on Robotics and Automation (ICRA)*, pages 4628–4634. IEEE, 2022. 6
- [26] Tianyu Li, Li Chen, Huijie Wang, Yang Li, Jiazhi Yang, Xiangwei Geng, Shengyin Jiang, Yuting Wang, Hang Xu, Chunjing Xu, et al. Graph-based topology reasoning for driving scenes. *arXiv preprint arXiv:2304.05277*, 2023. 6

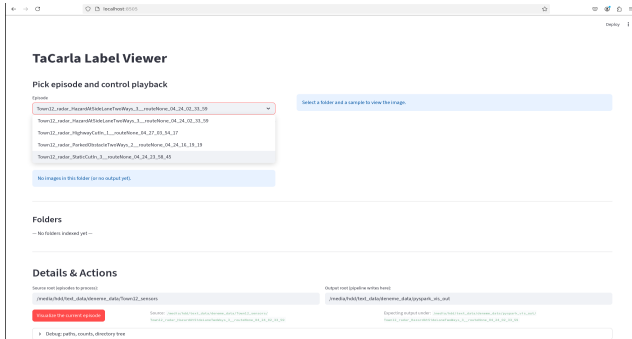
- [27] Zhiqi Li, Zhiding Yu, Shiyi Lan, Jiahao Li, Jan Kautz, Tong Lu, and Jose M. Alvarez. Is ego status all you need for open-loop end-to-end autonomous driving? In *2024 IEEE/CVF Conference on Computer Vision and Pattern Recognition (CVPR)*, pages 14864–14873, 2024. 4
- [28] Bencheng Liao, Shaoyu Chen, Haoran Yin, Bo Jiang, Cheng Wang, Sixu Yan, Xinbang Zhang, Xiangyu Li, Ying Zhang, Qian Zhang, and Xinggang Wang. Diffusiondrive: Truncated diffusion model for end-to-end autonomous driving. *arXiv preprint arXiv:2411.15139*, 2024. 7, 8
- [29] Bencheng Liao, Shaoyu Chen, Yunchi Zhang, Bo Jiang, Qian Zhang, Wenyu Liu, Chang Huang, and Xinggang Wang. Maptrv2: An end-to-end framework for online vectorized hd map construction. *International Journal of Computer Vision*, pages 1–23, 2024. 6
- [30] Tsung-Yi Lin, Michael Maire, Serge Belongie, James Hays, Pietro Perona, Deva Ramanan, Piotr Dollár, and C Lawrence Zitnick. Microsoft COCO: Common Objects in Context. In *The European Conference on Computer Vision (ECCV)*, 2014. 3, 7
- [31] Siddharth Mysore, Bassel Mabsout, Renato Mancuso, and Kate Saenko. Regularizing action policies for smooth control with reinforcement learning, 2021. 3
- [32] Dong-Hee Paek, Seung-Hyun Kong, and Kevin Tirta Wijaya. K-lane: Lidar lane dataset and benchmark for urban roads and highways. In *Proceedings of the IEEE/CVF Conference on Computer Vision and Pattern Recognition (CVPR) Workshop on Autonomous Driving (WAD)*, 2022. 3
- [33] Xingang Pan, Jianping Shi, Ping Luo, Xiaogang Wang, and Xiaoou Tang. Spatial as deep: Spatial cnn for traffic scene understanding. In *AAAI Conference on Artificial Intelligence (AAAI)*, 2018. 3
- [34] Jonah Philion and Sanja Fidler. Lift, splat, shoot: Encoding images from arbitrary camera rigs by implicitly unprojecting to 3d. In *Computer Vision—ECCV 2020: 16th European Conference, Glasgow, UK, August 23–28, 2020, Proceedings, Part XIV 16*, pages 194–210. Springer, 2020. 5
- [35] Mark Philip Philipsen, Morten Bornø Jensen, Andreas Møgelmo, Thomas B Moeslund, and Mohan M Trivedi. Traffic light detection: A learning algorithm and evaluations on challenging dataset. In *intelligent transportation systems (ITSC), 2015 IEEE 18th international conference on*, pages 2341–2345. IEEE, 2015. 3
- [36] Ilija Radosavovic, Raj Prateek Kosaraju, Ross Girshick, Kaiming He, and Piotr Dollár. Designing network design spaces. In *Proceedings of the IEEE/CVF conference on computer vision and pattern recognition*, pages 10428–10436, 2020. 5
- [37] K Renz, L Chen, AM Marcu, J Hünermann, B Hanotte, A Karnsund, J Shotton, E Arani, and O Sinavski. Carllava: Vision language models for camera-only closed-loop driving. arxiv 2024. *arXiv preprint arXiv:2406.10165*. 1
- [38] Katrin Renz, Kashyap Chitta, Otniel-Bogdan Mercea, A. Sophia Koepke, Zeynep Akata, and Andreas Geiger. Plant: Explainable planning transformers via object-level representations. In *Conference on Robotic Learning (CoRL)*, 2022. 7, 8, 1
- [39] Karen Spärck Jones. A statistical interpretation of term specificity and its application in retrieval. In *Journal of Documentation*, pages 11–21. Emerald Group Publishing, 1972. CiteSeerX 10.1.1.115.8343. 5
- [40] Bonifaz Stuhr, Johann Haselberger, and Julian Gebele. Carlane: A lane detection benchmark for unsupervised domain adaptation from simulation to multiple real-world domains. In *Advances in Neural Information Processing Systems*, pages 4046–4058. Curran Associates, Inc., 2022. 3
- [41] Pei Sun, Henrik Kretzschmar, Xerxes Dotiwalla, Aurelien Chouard, Vijaysai Patnaik, Paul Tsui, James Guo, Yin Zhou, Yuning Chai, Benjamin Caine, Vijay Vasudevan, Wei Han, Jiquan Ngiam, Hang Zhao, Aleksei Timofeev, Scott Ettinger, Maxim Krivokon, Amy Gao, Aditya Joshi, Yu Zhang, Jonathon Shlens, Zhifeng Chen, and Dragomir Anguelov. Scalability in perception for autonomous driving: Waymo open dataset. In *Proceedings of the IEEE/CVF Conference on Computer Vision and Pattern Recognition (CVPR)*, 2020. 2
- [42] Mingxing Tan, Ruoming Pang, and Quoc V Le. Efficientdet: Scalable and efficient object detection. In *Proceedings of the IEEE/CVF conference on computer vision and pattern recognition*, pages 10781–10790, 2020. 5
- [43] Zhi Tian, Chunhua Shen, Hao Chen, and Tong He. Fcos: Fully convolutional one-stage object detection. In *The IEEE International Conference on Computer Vision (ICCV)*, 2019. 7
- [44] Huijie Wang, Tianyu Li, Yang Li, Li Chen, Chonghao Sima, Zhenbo Liu, Bangjun Wang, Peijin Jia, Yuting Wang, Shengyin Jiang, et al. Openlane-v2: A topology reasoning benchmark for unified 3d hd mapping. *Advances in Neural Information Processing Systems*, 36, 2024. 3, 6
- [45] Benjamin Wilson, William Qi, Tanmay Agarwal, John Lambert, Jagjeet Singh, Siddhesh Khandelwal, Bowen Pan, Ratnesh Kumar, Andrew Hartnett, Jhony Kaesemodel Pontes, et al. Argoverse 2: Next generation datasets for self-driving perception and forecasting. *arXiv preprint arXiv:2301.00493*, 2023. 2
- [46] Dongming Wu, Jiahao Chang, Fan Jia, Yingfei Liu, Tiancai Wang, and Jianbing Shen. Topomlp: An simple yet strong pipeline for driving topology reasoning. *ICLR*, 2024. 6
- [47] Hang Xu, Shaoju Wang, Xinyue Cai, Wei Zhang, Xiaodan Liang, Li, and Zhenguo. Curvelane-nas: Unifying lane-sensitive architecture search and adaptive point blending. In *ECCV*, 2020. 3
- [48] Fan Yan, Ming Nie, Xinyue Cai, Jianhua Han, Hang Xu, Zhen Yang, Chaoqiang Ye, Yanwei Fu, Michael Bi Mi, and Li Zhang. Once-3dlanes: Building monocular 3d lane detection. In *Proceedings of the IEEE/CVF Conference on Computer Vision and Pattern Recognition*, 2022. 3
- [49] Tianwei Yin, Xingyi Zhou, and Philipp Krahenbuhl. Center-based 3d object detection and tracking. In *Proceedings of the IEEE/CVF conference on computer vision and pattern recognition*, pages 11784–11793, 2021. 5
- [50] Seungwoo Yoo, Heeseok Lee, Heesoo Myeong, Sungrack Yun, Hyoungwoo Park, Janghoon Cho, and Duck Hoon Kim. End-to-end lane marker detection via row-wise classification, 2020. 3

- [51] Fisher Yu, Haofeng Chen, Xin Wang, Wenqi Xian, Yingying Chen, Fangchen Liu, Vashisht Madhavan, and Trevor Darrell. Bdd100k: A diverse driving dataset for heterogeneous multitask learning. In *IEEE/CVF Conference on Computer Vision and Pattern Recognition (CVPR)*, 2020. [3](#)
- [52] Fisher Yu, Haofeng Chen, Xin Wang, Wenqi Xian, Yingying Chen, Fangchen Liu, Vashisht Madhavan, and Trevor Darrell. Bdd100k: A diverse driving dataset for heterogeneous multitask learning, 2020. [3](#)
- [53] Junrui Zhang, Chenjie Wang, Jie Peng, Haoyu Li, Jianmin Ji, Yu Zhang, and Yanyong Zhang. Cafe-ad: Cross-scenario adaptive feature enhancement for trajectory planning in autonomous driving, 2025. [3](#)
- [54] Tianyuan Zhang, Lu Wang, Hainan Li, Yisong Xiao, Siyuan Liang, Aishan Liu, Xianglong Liu, and Dacheng Tao. Lanevil: Benchmarking the robustness of lane detection to environmental illusions, 2024. [3](#)
- [55] Yujun Zhang, Lei Zhu, Wei Feng, Huazhu Fu, Mingqian Wang, Qingxia Li, Cheng Li, and Song Wang. Vil-100: A new dataset and a baseline model for video instance lane detection, 2021. [3](#)

6. Supplementary

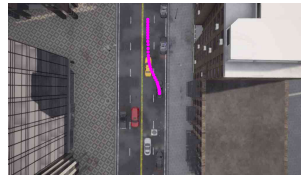
6.1. Annotation Details

Samples in TaCarla were collected using the PlanT [38] data pipeline. An additional translation is applied to compensate for the virtual ego-vehicle center (1.3 m in x , 2.5 m in z). All labels are stored as Parquet files, which can be read with PySpark to reduce label loading time. In addition, we provide code for reading labels from Parquet files, making it easier for others to use the dataset.



6.2. Scenarios

The scenarios are arranged in the CARLA 9.15 simulator to increase diversity for learning-based planning. Unlike Leaderboard 1.0, Leaderboard 2.0 requires learning overtaking, stopping, merging, and avoiding dynamic actors. The following figures illustrate each scenario. Pink waypoints show future ego positions (8–30 frames ahead), warped to the current coordinate frame.



Accident: Ego overtakes parked multiple vehicles.



AccidentTwoWays: Overtaking parked multiple vehicles into the opposite lane.



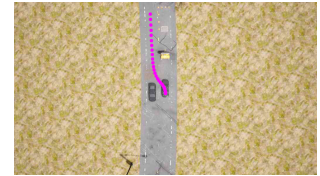
BlockedIntersection: Intersection blocked.



ControlLoss: Temporary loss of vehicle control.



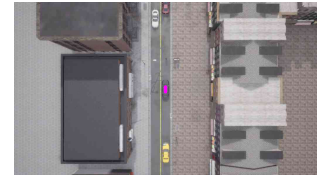
ConstructionObstacle: Lane blocked by construction.



ConstructionObstacleTwoWays: Overtaking via oncoming lane.



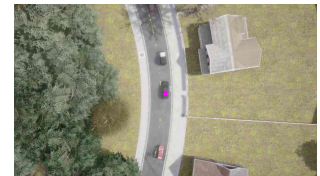
CrossingBicycleFlow: Bicycles crossing the junction.



DynamicObjectCrossing / PedestrianCrossing: Pedestrian or cyclist crossing.



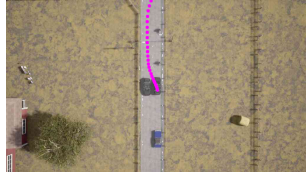
EnterActorFlow/V2: Joining a main road with traffic flow.



HardBrakeRoute: Sudden stop of lead vehicle.



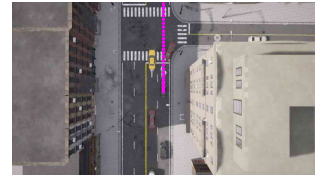
HazardAtSideLane: Slow bicycles on roadside.



HazardAtSideLaneTwoWays: Overtaking bicycles via opposite lane.



ParkingExit: Ego exits a parking spot.



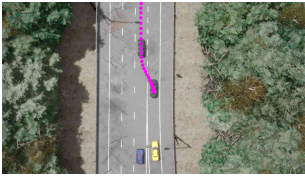
PriorityAtJunction: Ego is prioritized to pass.



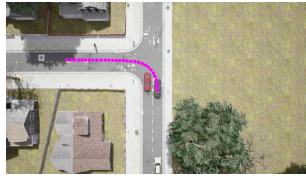
HighwayCutIn: Another vehicle cuts in.



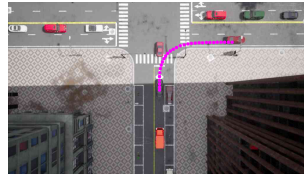
InterurbanActor-Flow/Advanced: Dense intersection flow.



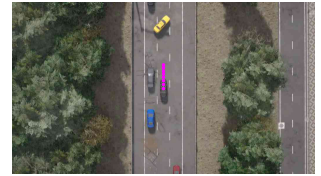
MergingIntoSlowTraffic: Merging onto slow-moving road.



NonSignalizedJunction-Left/RightTurn: Turning without traffic lights.



SignalizedJunction-Left/RightTurn: Turns at signalized junction.



StaticCutIn: Stationary vehicle suddenly cuts in.



OppositeVehicleRunningRed-Light/TakingPriority.



ParkedObstacle/TwoWays: Overtaking a parked vehicle.



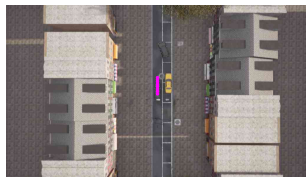
VehicleTurningRoute/ Pedestrian: Pedestrian during turning.



YieldToEmergencyVehicle: Ego yields to emergency vehicle.



ParkingCrossingPedestrian: Pedestrian emerging from behind a vehicle.



ParkingCutIn: Parked vehicle suddenly merges.

Table 9. Open-loop metrics (ADE ↓, FDE ↓, AHE ↓, FHE ↓) for each scenario.

Scenario Name	Model	ADE ↓	FDE ↓	AHE ↓	FHE ↓	Scenario Name	Model	ADE ↓	FDE ↓	AHE ↓	FHE ↓
Accident	DiffusionDrive	2.1493	4.0263	0.1040	0.1156	OppositeVehicleRunningRedlight	DiffusionDrive	1.6435	3.1160	0.0324	0.0364
	PlanT	1.4002	2.2346	0.1368	0.1934		PlanT	1.3400	2.1328	0.0350	0.0178
	Transfuser	1.8716	3.4446	0.1109	0.0963		Transfuser	1.3820	2.6198	0.0085	0.0074
AccidentTwoWays	DiffusionDrive	0.8104	1.5032	0.6924	0.6760	OppositeVehicleTakingPriority	DiffusionDrive	0.8963	1.6087	0.0521	0.0491
	PlanT	0.5810	2.2346	0.1368	0.1934		PlanT	1.7681	2.9627	0.0265	0.0231
	Transfuser	0.5422	1.0367	0.8329	1.0033		Transfuser	0.8336	1.5672	0.0156	0.0157
BlockedIntersection	DiffusionDrive	1.0451	1.9725	0.4265	0.4387	ParkedObstacle	DiffusionDrive	3.8699	7.3543	0.0734	0.0995
	PlanT	1.2397	2.0076	0.6148	0.8359		PlanT	1.6408	2.6752	0.2131	0.1079
	Transfuser	1.1008	2.1835	0.4541	0.5256		Transfuser	2.9464	5.6412	0.0278	0.0309
ConstructionObstacleTwoWays	DiffusionDrive	0.7603	1.4043	0.6028	0.6724	ParkedObstacleTwoWays	DiffusionDrive	0.8414	1.5375	0.2680	0.2518
	PlanT	2.8932	4.9572	0.0632	0.0806		PlanT	0.7499	1.2404	0.2798	0.2334
	Transfuser	0.4308	0.7822	0.7733	1.0419		Transfuser	0.6938	1.2970	0.2149	0.2156
ControlLoss	DiffusionDrive	0.8896	1.6741	0.1025	0.1024	ParkingCrossingPedestrian	DiffusionDrive	0.7730	1.3273	0.3226	0.3002
	PlanT	0.5790	0.9722	0.1924	0.2077		PlanT	0.7523	1.1728	0.5261	0.4350
	Transfuser	0.5935	1.1126	0.0787	0.0853		Transfuser	0.5847	1.0419	0.4454	0.6068
DynamicObjectCrossing	DiffusionDrive	0.9871	1.8262	0.1476	0.1331	ParkingCutIn	DiffusionDrive	0.8182	1.4240	0.4070	0.3682
	PlanT	0.9846	1.5602	0.3478	0.3785		PlanT	0.6404	0.9740	0.6235	0.5215
	Transfuser	0.8131	1.5747	0.1357	0.1465		Transfuser	0.8151	1.4573	0.4517	0.5596
EnterActorFlow	DiffusionDrive	1.1639	2.2517	0.0301	0.0411	ParkingExit	DiffusionDrive	1.4377	2.7670	0.2318	0.2468
	PlanT	1.6695	2.7945	0.0224	0.0246		PlanT	0.5360	0.9217	0.5211	0.2358
	Transfuser	1.2159	2.2782	0.0302	0.0357		Transfuser	1.0385	1.9858	0.1538	0.1154
HardBreakRoute	DiffusionDrive	0.9202	1.7693	0.3500	0.3283	PedestrianCrossing	DiffusionDrive	1.8471	3.7742	0.1810	0.1688
	PlanT	0.3669	0.6509	0.5425	0.4152		PlanT	1.7926	3.0981	0.6149	0.4200
	Transfuser	0.8418	1.6670	0.3553	0.2879		Transfuser	1.2441	2.5625	0.3430	0.3743
HazardAtSideLane	DiffusionDrive	1.8221	3.4470	0.0961	0.1010	PriorityAtJunction	DiffusionDrive	0.6663	1.1983	0.1608	0.1718
	PlanT	2.3169	3.7521	0.1863	0.1486		PlanT	0.4824	0.7867	0.2022	0.2208
	Transfuser	1.8582	3.5167	0.0875	0.0902		Transfuser	0.6363	1.1397	0.2277	0.2609
HazardAtSideLaneTwoWays	DiffusionDrive	1.2479	2.4540	0.0458	0.0490	SignalizedJunctionLeftTurn	DiffusionDrive	2.1807	4.2420	0.2154	0.2378
	PlanT	1.8753	3.2281	0.0328	0.0347		PlanT	2.1885	3.6065	0.2567	0.2515
	Transfuser	0.9637	1.8608	0.0225	0.0294		Transfuser	1.5983	3.1293	0.1678	0.2216
HighwayExit	DiffusionDrive	1.3126	2.5442	0.0373	0.0422	SignalizedJunctionRightTurn	DiffusionDrive	1.7408	3.2851	0.1120	0.1567
	PlanT	1.1354	1.9507	0.0620	0.0709		PlanT	1.6994	2.8513	0.1602	0.1629
	Transfuser	1.0215	1.9594	0.0439	0.0355		Transfuser	1.5451	2.9369	0.1474	0.1570
MergerIntoSlowTraffic	DiffusionDrive	2.4493	4.5116	0.0762	0.0851	StaticCutIn	DiffusionDrive	1.7001	3.2323	0.1431	0.1204
	PlanT	3.1610	5.2284	0.1672	0.1563		PlanT	0.9219	1.5490	0.3423	0.3070
	Transfuser	1.8243	3.3578	0.0638	0.0779		Transfuser	1.1787	2.2042	0.1716	0.2178
MergerIntoSlowTrafficV2	DiffusionDrive	1.9542	3.6690	0.1677	0.1683	VehicleTurningRoute	DiffusionDrive	1.0698	1.9596	0.2788	0.2660
	PlanT	1.8335	3.1872	0.1761	0.1634		PlanT	1.0357	1.7030	0.5682	0.6189
	Transfuser	1.9213	3.8040	0.1369	0.1280		Transfuser	0.9895	1.8191	0.3002	0.4327
NonSignalizedJunctionLeftTurn	DiffusionDrive	1.3052	2.4879	0.1387	0.1602	VehicleTurningRoutePedestrian	DiffusionDrive	1.0859	2.0227	0.2285	0.2530
	PlanT	1.4098	2.3628	0.1842	0.2272		PlanT	0.8221	1.3853	0.6458	0.7563
	Transfuser	1.1051	2.1444	0.1293	0.1526		Transfuser	0.8494	1.6047	0.2154	0.2058
NonSignalizedJunctionRightTurn	DiffusionDrive	1.6663	3.3112	0.1150	0.1305	YieldToEmergencyVehicle	DiffusionDrive	1.4413	3.0138	0.0252	0.0244
	PlanT	1.8390	3.1044	0.2153	0.2461		PlanT	1.5263	2.5886	0.0889	0.1030
	Transfuser	1.3446	2.6837	0.1063	0.1106		Transfuser	0.6925	1.3326	0.0164	0.0214